arXiv:1208.1396v1 [quant-ph] 7 Aug 2012

Fidelity of qubit rotations in the presence of thermal motion

Anat Daniel, Ruti Agou, Omer Amit, David Groswasser, Yonathan Japha and Ron Folman*
Ben-Gurion University of the Negev
(Dated: August 8, 2012)

We investigate both theoretically and experimentally the effect of real-life imperfections on the fidelity of qubit rotations in the presence of thermal motion. Specifically we develop a model predicting the coherence time of Rabi oscillations in the presence of an inhomogeneous driving field or Ramsey oscillations in the presence of an inhomogeneous state-selective potential. We demonstrate the theoretical dependence by an experiment observing the coherence time in a volume much smaller than the entire sample.

PACS numbers: 37.10.Gh, 32.70.Cs, 05.40.-a, 67.85.-d

Since the middle of the previous century, the two-level system has been the source of numerous new theoretical and experimental insights into the basic tenets of quantum theory. Later on, the two-level system has become the main building block of numerous applications ranging from clocks [1] and magnetic sensors [2] to quantum communications [3] and computing [4]. Recently, this two-level system has been named the qubit. Understanding the sources of errors when manipulating this system is of paramount importance for technological applications as well as fundamental studies [5].

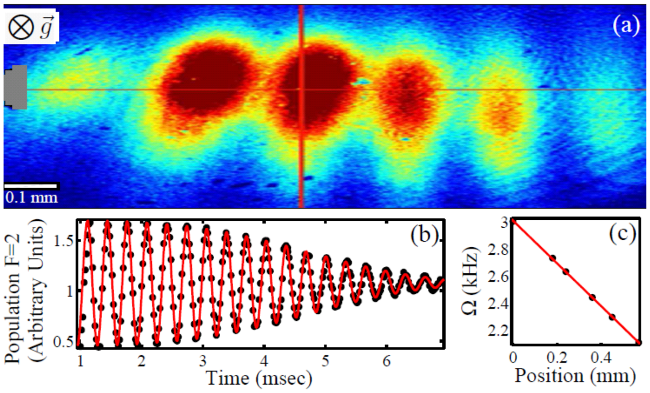

FIG. 1: (color online) (a) absorption image of ^{87}Rb atoms at the $F = 2$ energy level after applying a spatially inhomogeneous MW field ($T = 43\ \mu$K). The image is taken while in free fall and the observed spatial axes are perpendicular to the gravitational axis. The MW horn antenna (depicted) radiates electromagnetic waves with decreasing amplitude as a function of distance, thus generating along the cloud multiple Rabi oscillations which can be viewed simultaneously, thereby creating a fringe-like pattern. (b) Rabi oscillations measured 10 cm away from the antenna [e.g. along the vertical line in (a)]. Each data point represents the same pixels in the cloud at different MW pulse durations. The coherence decay is due to the gradient of the MW field and the velocity of the atoms (temperature). (c) The plot shows the dependence of the observed Rabi frequency on the position across the cloud where the origin of the graph refers to the center of the cloud. The data was fitted to a linear curve and results with $\partial_x\Omega = -1.742 \pm 0.129$ $[1/msec \cdot mm]$.

The manipulation and evolution of such a two-level system, defined in quantum theory as $|\psi\rangle = a|1\rangle + b|2\rangle$, is perhaps best described by a vector on the Bloch sphere defined by angles θ and ϕ, where $a = \cos\frac{\theta}{2}$ and $b = \sin\frac{\theta}{2}e^{i\phi}$. In a stationary situation the two qubit states may be chosen as energy eigenstates and then $\phi = -(E_2 - E_1)t/\hbar$ (E_i being the energy of state i). Any manipulation of the qubit state is typically called a rotation as it rotates the state vector on the sphere. For example, in the presence of an oscillating driving field resonant with the energy $E_2 - E_1$ the angle θ rotates as $\theta = \Omega t$, where the Rabi frequency Ω is proportional to the amplitude of the driving field. The fidelity of a single-qubit operation is defined as the overlap of the actual final state with the target state.

In real-life devices, gradients of static fields (determining $E_2 - E_1$) or driving fields unfortunately exist (field gradients are an experimental reality even if cavities are used [6, 7]). In such a case, there exists a first order broadening effect which reduces the coherence time. This may be viewed in Fig. 1(a), where a gradient of a driving micro-wave (MW) field induces multiple Rabi frequencies in space. This is true also for a sample temperature of $T = 0$. However, when $T \neq 0$ a second order decoherence effect appears, as atoms move between different Rabi frequency regions. This decrease may be observed by studying the Rabi oscillations in a small volume element, much smaller than the sample size [Fig. 1(b)]. It is this second order effect which is the topic of this paper.

We investigate both theoretically and experimentally the reduction in fidelity in a small volume element as a function of atom temperature and field gradient. The significance of the small volume element fidelity goes beyond fundamental interest; it may also be of practical importance, for example, in the optimization of signal to noise in situations in which the coherence time is more dominant than the number of atoms, or when, for technical reasons, imaging a volume smaller than the trap size, e.g. when utilizing near field optics as enabled by atom chips [8–11]. Next, we calculate the fidelity of the common rotation of $\theta = 90^o$, typically called a $\pi/2$ pulse. Finally, we show that our model may be expanded to describe any trapped system in which both qubit states feel the same potential (e.g. $|F, m_F\rangle = |1, -1\rangle$ and $|2, 1\rangle$ [14]), or systems with arbitrary qubit states where a constant potential is used i.e. box potentials (e.g. [15]). Such traps may be used in the future for a wide variety of applications (e.g. quantum computers) as they reduce potential induced inhomogeneities. Our results may be used to improve the fidelity of such systems.

The model system we are analyzing in this paper is that of freely propagating atoms when no potential is applied. We first construct a theoretical model which is solved both analytically and numerically, and then experimentally demonstrate the consequences of the model. Our experiment utilizes a far field MW imaging method presented here for the first time [12] [Fig. 1(a)]. A similar near-field method was developed independently by the Treutlein group [13].

Our theoretical model assumes an ensemble of two-level atoms whose motional degrees of freedom evolve classically in time and are given initially by a classical distribution $P(\mathbf{x}, \mathbf{v})$ in position and velocity space. The internal state of an atom with an initial position $\mathbf{x}_0$ and velocity $\mathbf{v}_0$ is generally given by

$$|\psi_{\mathbf{x}_0,\mathbf{v}_0}(t)\rangle = a_{\mathbf{x}_0,\mathbf{v}_0}(t)|1\rangle + e^{-i\omega_{12}t} b_{\mathbf{x}_0,\mathbf{v}_0}(t)|2\rangle, \tag{1}$$

where $\omega_{12} = (E_2 - E_1)/\hbar$ is the transition frequency. The equations of motion for the evolution of the internal state under the influence of an applied radiation field are

$$\begin{aligned} \dot{a}_{\mathbf{x}_0,\mathbf{v}_0} &= -\frac{i}{2} e^{i(\omega-\omega_{12})t} \Omega[\mathbf{x}(\mathbf{x}_0, \mathbf{v}_0, t)] b_{\mathbf{x}_0,\mathbf{v}_0} \\ \dot{b}_{\mathbf{x}_0,\mathbf{v}_0} &= -\frac{i}{2} e^{-i(\omega-\omega_{12})t} \Omega[\mathbf{x}(\mathbf{x}_0, \mathbf{v}_0, t)]^* a_{\mathbf{x}_0,\mathbf{v}_0}, \end{aligned} \tag{2}$$

where ω is the frequency of the driving field, and $\Omega(\mathbf{x})$ is the Rabi frequency for qubit rotation at a given point $\mathbf{x}(\mathbf{x}_0, \mathbf{v}_0, t)$ along the atomic trajectory, which is proportional to the amplitude of the driving field at that point. As the driving field is usually in the microwave frequency regime, we may ignore the Doppler shift and assume a constant frequency for all velocities.

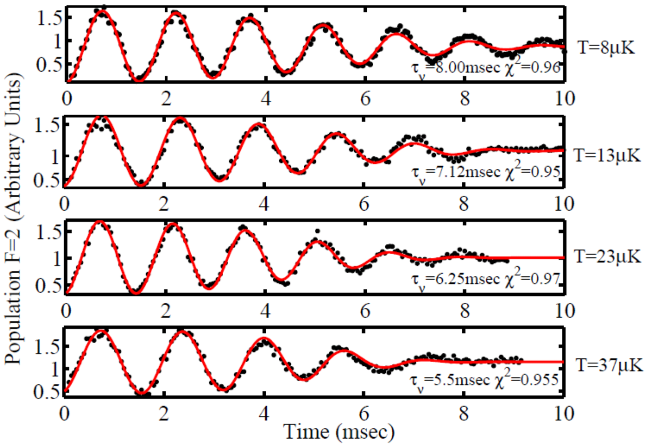

FIG. 2: (color online) Rabi oscillations for different temperatures (8 μK to 37 μK). The graphs present the normalized population in $F = 2$ as a function of the MW pulse duration. It can be seen that the coherence time of the oscillations increases when the temperature decreases. Each of the graphs was fitted to the model of Eq. (10) (see text for more details). The resulting τ_v and χ^2 are shown.

Once Eqs. (2) are solved for every trajectory, the density matrix for the internal state is given by an integral over the initial external degrees of freedom of the atoms

$$\begin{aligned} \rho_{ij}(\mathbf{x}, t) &= \int d^3\mathbf{x}_0 \int d^3\mathbf{v}_0 P(\mathbf{x}_0, \mathbf{v}_0) \delta^3[\mathbf{x} - \mathbf{x}(\mathbf{x}_0, \mathbf{v}_0, t)] \times \\ &\quad \times \langle i|\psi_{\mathbf{x}_0,\mathbf{v}_0}(t)\rangle\langle\psi_{\mathbf{x}_0,\mathbf{v}_0}(t)|j\rangle \end{aligned} \tag{3}$$

for $i, j = 1, 2$, such that $\langle 1|\psi\rangle = a$ and $\langle 2|\psi\rangle = b$.

A simple analytic solution for Eqs. (2) may be obtained for the case where the driving field is resonant with the atomic frequency ω_{12}. Then the Rabi frequency Ω may be chosen to be real. In this case we obtain the solution

$$\begin{aligned} a(t) &= \cos[\xi(t)]a(0) - i\sin[\xi(t)]b(0) \\ b(t) &= -i\sin[\xi(t)]a(0) + \cos[\xi(t)]b(0), \end{aligned} \tag{4}$$

where $\xi(t) = \frac{1}{2}\int_0^t dt'\Omega(t')$.

First we consider the simple case which applies to the conditions of our experiment, as described below. We assume a free collisionless motion during the time where the radiation is applied, such that the velocity $\mathbf{v}$ of a particle remains equal to the initial velocity $\mathbf{v}_0$ and $\mathbf{x}(\mathbf{x}_0, \mathbf{v}, t) = \mathbf{x}_0 + \mathbf{v}t$. We also assume that the distances $|\mathbf{v}|t$ traversed by the atoms are smaller than the size of the initial atomic cloud. We further assume a small field variation such that over these distances

$$\Omega(\mathbf{x}) \approx \Omega_0 + (\nabla\Omega) \cdot (\mathbf{x} - \mathbf{x_c}) \tag{5}$$

where $\nabla\Omega$ is a constant gradient and Ω_0 is the Rabi frequency at a given central point $\mathbf{x}_c$. In this case the phase $\xi(t)$ in Eq. (4) is

$$\xi_{\mathbf{v}}(\mathbf{x}, t) = \frac{1}{2}\Omega(\mathbf{x})t - \frac{1}{4}\mathbf{v} \cdot (\nabla\Omega)t^2, \tag{6}$$

where $\Omega(\mathbf{x})$ is the Rabi frequency at the observation point. As only the velocity component along the direction of the field gradient affects the internal atomic dynamics, we take this direction to be denoted by x and refer to v_x as v. Assuming a Boltzmann distribution of the atomic velocity

$$P(v) = \sqrt{\frac{m}{2\pi k_B T}} \exp\left[-\frac{mv^2}{2k_B T}\right], \tag{7}$$

and taking the atoms to be initially at state $|1\rangle$, we find, using Eq. (3), that the population of the state $|2\rangle$ is

$$\begin{aligned} n_2(x) &= \rho_{22}(x) = \int_{-\infty}^{\infty} dv\ P(v)\sin^2[\xi_v(x, t)] \\ &= \frac{1}{2}\left[1 - \cos\Omega(x)t \exp[-t^4(\partial_x\Omega)^2 k_B T/8m]\right] \end{aligned} \tag{8}$$

where we have used $\sin^2\xi = (1-\cos 2\xi)/2$. It follows that the amplitude of Rabi oscillations decays as $\exp[-(t/\tau_v)^4]$, where the temperature dependent coherence time is

$$\tau_v = \frac{8^{1/4}}{(\bar{v}|\partial_x\Omega|)^{1/2}}, \tag{9}$$

with $\bar{v} = \sqrt{\langle v^2\rangle} = \sqrt{k_BT/m}$ being the average velocity.

If the imaging system which probes the state of the atoms at a given point has a finite resolution, such that every pixel of the camera represents a convolution of the atomic density at a given point with a Gaussian function $(\sqrt{\pi}\sigma_I)^{-1}\exp[-(x-x')^2/2\sigma_I^2]$ of radius σ_I due to imaging limitations, then the number of atoms at level $|2\rangle$ is

$$n_2(x,t) = \frac{1}{2}\left\{1-\cos[\Omega(x)t]\exp[-(t/\tau_x)^2-(t/\tau_v)^4]\right\}, \tag{10}$$

where

$$\tau_x = \frac{2^{1/2}}{\sigma_I(\partial_x\Omega)}. \tag{11}$$

This integration over a finite spatial range represents the ordinary decoherence effect of the spatial inhomogeneity.

To demonstrate the theoretical model we experimentally investigate a cloud of freely propagating atoms (in free-fall). We start our experiment with a cloud of 10^6 cold ^{87}Rb atoms. The atoms are cooled by a standard Magneto-Optical-Trap (MOT) followed by laser molasses to the required temperature, down to a few μK. The atoms are prepared in the $F=1$ state. To avoid inhomogeneities, the atoms are then released into free-fall for the duration of the experiment, typically $10-30$ ms. During the free-fall the atoms are subjected for a time t, via a horn antenna, to a MW field tuned at 6.8 GHz to the $|F,m_F\rangle = |1,0\rangle \equiv |1\rangle \rightarrow |2,0\rangle \equiv |2\rangle$ transition. After time t the MW field is switched off and the population of the atoms in the $F=2$ state is determined by on resonance absorption imaging directed along the gravitational axis. The MW field induces Rabi oscillations, the coherence time of which we analyze.

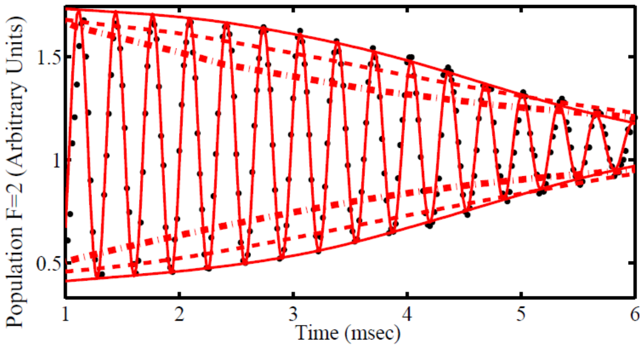

FIG. 3: (color online) A comparison of fitting different models to the data ($T = 43\mu K$). The dotted, dashed and solid lines present the envelope of the exponential (t) model, the Gaussian (t^2) model and our model presented in Eq. (10), respectively. The latter model returns a χ^2 value of 0.972, while the Gaussian model returns $\chi^2 = 0.947$ and the exponential model returns $\chi^2 = 0.844$.

In Fig. 1(a) we present a typical experimental image following the sequence described above. As the horn antenna produces a spatially inhomogeneous MW field, a gradient of Rabi frequencies is produced along the cloud (decreasing frequency with growing distance from the antenna); this is exhibited in the figure as a fringe-like pattern [12]. In Fig. 1(b) we present a typical Rabi oscillation plot ($F=2$ population vs. t) as seen in the data taken from a vertical strip of pixels one pixel wide and 100 pixels long (perpendicular to the direction of the field gradient). One may deduce the gradient by fitting the spatial dependence of the measured Rabi frequencies to a linear slope. Far away from the antenna one may assume a nearly linear slope as one expects the magnetic field radiated by the antenna to fall as $1/r$ [Fig. 1(c)].

Next, we analyze the coherence time as a function of temperature. In Fig. 2 we present as an example four data sets of Rabi oscillations at different temperatures. The model presented in Eq. (10) fits well to the data. To make the fit, we insert into Eq. (10) an arbitrary constant phase to account for possible systematic shifts in the timing of the experiment, so that the fit is to the

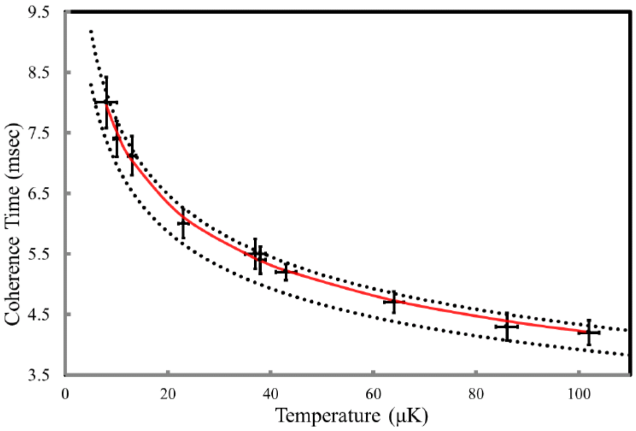

FIG. 4: (color online) Coherence time as a function of the temperature ($T = 8-102\ \mu$K). The data points are the coherence time extracted from the t^4 model, fitted to the data as shown in Fig. 2. The temperatures were measured using time-of flight (TOF). The error values of the coherence time and temperature were calculated in the model with a confidence level of 95%. The data points of coherence time (τ_v) for each temperature (T) were then fitted to the model presented in Eq. (9) and the fit returns a χ^2 value of 0.996. The region between the dotted lines indicates the range of the predicted theoretical values taking into account the errors on the measured Rabi frequency gradient. This confirms to a high level of confidence our theoretical model.

function $f(t) = A\exp[-(t/\tau_x)^2-(t/\tau_v)^4]\cos(\Omega t+\phi)+B$. The A and B constants are added because the oscillation amplitude and the average are not exactly known. In addition, to make the fit, we first need to estimate τ_x. When leaving both τ_x and τ_v as free parameters, a fit on the $T = 43$ μK data set appearing in Fig. 1(b), returns $\tau_x = 8.8$ msec with a χ^2 of 0.97. This corresponds to σ_I of 94 microns [Eq. (11), with $\partial_x\Omega = 1.7$ (mm msec)$^{-1}$ from Fig. 1(c)] which in turn corresponds to a misalignment of our 30 cm focal length lens by 1 mm or so along the imaging axis. As we estimate that our optics alignment error is at least that (as the cloud size itself is about 1 mm in all directions), we adopt in the following the $\tau_x = 8.8$ msec value [Eq. (11)] in the rest of the paper and leave only τ_v as a free parameter. Let us note that the procedure is very robust and changing σ_I by a factor of 2 in each direction returns χ^2 values with a mere change of 1%. Finally, we also fit the data to Eq. (10) while replacing the power of 4 by a free parameter d and find that it converges to values of $d = 3.778 - 4.1$ with χ^2 values $0.961 - 0.971$.

For comparison we plot in Fig. 3 one set of Rabi oscillations ($T = 43$ μK) with a fit to three possible models: a Gaussian model, an exponential model and the t^4 model. One can clearly see that the t^4 model better fits the data by far. We now use the gradient measured by the fit presented in Fig. 1(c) to compare the observed coherence times at different temperatures to the theoretically expected value. As presented in Fig. 4, the data fits well with the theoretical prediction.

The t^4 exponential dependence of the decay of Rabi oscillations follows from the Gaussian velocity distribution in the thermal cloud. Atoms with higher velocity travel a larger distance along the field gradient thereby acquiring a larger phase difference relative to atoms at rest in the detection point. This additional phase is an integral over time along the way which was traversed by an atom with a given velocity, which is vt, such that the total phase depends quadratically on time. The combination of the quadratic dependence of the phase on time and the quadratic exponential dependence of the distribution on velocity provides the t^4 quadratic dependence of the coherence on time. We may consider τ_v as a critical time such that at smaller times the qubit rotation is unaffected by the velocity.

Finally, we use the t^4 model to infer the fidelity of a $\pi/2$ pulse. Fidelity is defined by the overlap between a target state $|\psi\rangle_{\rm target}$ and an actual state $|\psi\rangle$. If the actual state is not pure then it is described by a density matrix $\rho = \sum_j w_j|\psi_j\rangle\langle\psi_j|$. The fidelity is then given by $F = \left[\sum_j w_j|\langle\psi_j|\psi\rangle_{\rm target}|^2\right]^{1/2}$. For a $\pi/2$ pulse the target state is $|\psi\rangle_{\rm target} = \cos(\pi/4)|1\rangle - i\sin(\pi/4)|2\rangle$. For a given velocity the actual state is $|\psi_v\rangle = \cos\left(\frac{1}{4}(\pi+\partial_x\Omega v t_0^2)\right)|1\rangle - i\sin\left[\frac{1}{4}(\pi+\partial_x\Omega v t_0^2)\right]|2\rangle$, where $t_0 = \pi/4\Omega_0$. The overlap between the actual state and the target state is $\langle\psi_v|\psi\rangle_{\rm target} = \cos(v\partial_x\Omega t_0^2/4)$. Integrating the square of the overlap over the different velocities we obtain $F^2 = \int dv P(v)|\langle\psi_v|\psi_{\rm target}\rangle|^2 = \frac{1}{2}\left\{1+\exp[-(\pi/4\Omega_0\tau_v)^4]\right\}$. When $\Omega_0\tau_v > \pi/4$ the fidelity is almost 1, while if $\Omega_0\tau_v < \pi/4$ the fidelity drops to a minimum value of $F = 1/\sqrt{2}$, which represents the fidelity for a totally random actual qubit state.

Note that an analysis similar to the one presented above for the effect of a gradient of a driving field applies also to a gradient of a stationary field when no driving field is applied. Such a stationary field consists a local differential potential $V(\mathbf{x})$ for the two levels, such that their mutual phase ϕ has a local term $\phi(\mathbf{x}) = -V(\mathbf{x})t/\hbar$. In this case the local coherence between the two levels is

$$\begin{aligned}\rho_{12}(\mathbf{x}) &= a(0)b^*(0)e^{i\omega_{12}t}\int d^3\mathbf{v}\,P(\mathbf{x},\mathbf{v})\times\\ &\times\exp\left[-\frac{i}{\hbar}\int_0^t dt' V[\mathbf{x}(t')]\right], \qquad (12)\end{aligned}$$

resulting in coherence times similar to τ_v and τ_x above, with the replacement $\nabla\Omega \to \nabla V/\hbar$. This result makes the analysis above relevant to situations such as the dark time in a Ramsey process in, for example, atomic clocks.

As an outlook we note that our model is relevant also to systems in which both qubit states feel the same potential, or in which for arbitrary qubit states the potential is constant. As is many times the case, when the position dependent interaction with the environment is stronger than the energy dependent interaction [16] and consequently the position base coherence time is smaller than the energy base coherence time, potentials are expected to house classical particles in the sense of external

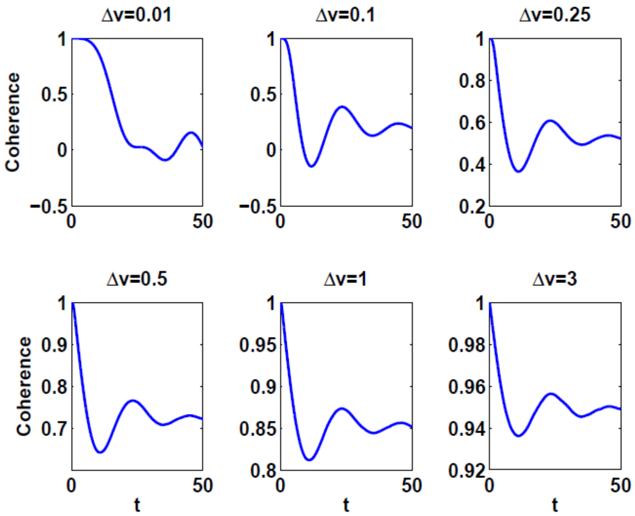

FIG. 5: (color online) Numerical simulation: Coherence of Rabi oscillations in the middle of a box trap with length L and a driving field gradient along the same axis, as a function of velocity spread Δv [units of L/(arb. time units)]. The gradient is $\partial_x\Omega = 0.1$ [units of 1/(L· arb. time units)].

degrees of freedom and quantum particles as far as the internal degrees of freedom are concerned [17]. Thus our model which is based on classical dynamics should also apply to trapped particles (as well a single trapped particle). As an example we analyze in the following a box potential (for which the above model for freely propagating atoms may be taken as the limit of a very large box). To adapt our model to box potentials one has to take into account the reflections at the walls. Our numerical study which will be presented elsewhere shows that indeed the coherence initially drops like $\exp\left(-\alpha\bar{v}^2t^4\right)$ at short times such that $t < L/\bar{v}$ (where L is the size of the box). For longer times, the addition of the walls adds the following behavior: The coherence time reaches a minimum value and oscillates around this value with decreasing oscillation. Eventually it stabilizes around a constant value which grows with velocity and is high when $|\bar{v}|\tau_v \gg L$ (τ_v being the coherence time for $L \to \infty$). This is presented in Fig. 5. Higher velocities give higher coherence for longer times because higher velocities correspond to paths with multiple reflections so that the field gradient is averaged out. This may be understood by making an analogy between the reflections at the walls and multiple π echo pulses in the middle of a Ramsey sequence [18]. An analogy can also be made to motional and collisional narrowing [19]. Hence the walls in fact simply add motional or collisional narrowing. However, if the population of a certain qubit level over the whole area of the box is probed, then the coherence functions in Fig. 5 must be multiplied by the spatial integration factor as in Eq. (10), which is, in our case, $\sin(\partial_x\Omega Lt)/(\partial_x\Omega Lt)$, corresponding to a decoherence due to ordinary inhomogeneous broadening $\tau_x = (\partial_x\Omega L)^{-1}$.

To conclude, we have shown that gradients of DC or AC fields reduce the coherence of qubit rotations both directly though an inhomogeneous rotation frequency and through a second order temperature dependent effect due to particle motion. We have demonstrated our theoretical model by a simple experimental system of freely falling atoms and also by a numerical example of a particle in a box. Our results may be useful to improve the operation of quantum devices.

We gratefully acknowledge help from the members of the atom chip group and especially, Amir Waxman, Shimon Machluf, Menachem Givon and Zina Binshtok.

---

[*] Electronic address: folman@bgu.ac.il

[1] M.A. Lombardi, T.P. Heavner, S.R. Jefferts, NIST Primary Frequency Standards and the Realization of the SI Second, Journal of Measurement Science **2**, 74 (2007).

[2] T.H. Sander, J. Preusser, R. Mhaskar, J. Kitching, L. Trahms and S. Knappe. Magnetoencephalography with a chip-scale atomic magnetometer. Biomedical Optics Express **3**, 981 (2012).

[3] Nicolas Gisin and Ron Thew, Quantum communication, Nature Photonics **1**, 165 (2007).

[4] T. D. Ladd, F. Jelezko, R. Laflamme, Y. Nakamura, C. Monroe and J. L. OBrien, Quantum computers, Nature **464**, 45 (2010).

[5] Worawarong Rakreungdet, Jae Hoon Lee, Kim Fook Lee, Brian E. Mischuck, Enrique Montano, and Poul S. Jessen, Accurate microwave control and real-time diagnostics of neutral-atom qubits, Physical Review A **79**, 022316 (2009).

[6] Li Ruoxin, Ph.D. Thesis, Phase variations in microwave cavities for atomic clocks, YALE UNIVERSITY (2007).

[7] Stella Torres Müller, Daniel Varela Magalhaes, Renato Ferracini Alves and Vanderlei Salvador Bagnato1, Compact Frequency Standard Based on an Intra-cavity Sample Cold Cesium Atoms, JOSA B **28**, 2592 (2011).

[8] R. Folman, P. Krüger, J. Schmiedmayer, J. Denschlag and C. Henkel, Controlling cold atoms using nanofabricated surfaces: Atom Chips, Adv. At. Mol. Opt. Phys. **48**, 263 (2002).

[9] J. Reichel, Microchip traps and BoseEinstein condensation, Appl. Phys. B **75**, 469 (2002).

[10] J. Fortágh and C. Zimmermann, Magnetic microtraps for ultracold atoms, Rev. Mod. Phys. **79**, 235 (2007).

[11] J. Reichel and V. Vuletic (Eds.), *Atom Chips*, Wiley-VCH, Berlin (2011).

[12] The position dependent Rabi phase, giving rise to fringes accross a cold atom cloud when it is exposed to MW radiation with an amplitude having a spatial gradient has been previously observed. See our work: Ruti Agou, M.Sc. Thesis, Microwave Manipulation of Cold Atoms (2011), `www.bgu.ac.il/atomchip/Theses/Ruti_Agou_MSc_2011.pdf`.

[13] P. Böhi et al., App. Phys. Lett. **97**, 051101 (2010).

[14] Philipp Treutlein, Peter Hommelhoff, Tilo Steinmetz, Theodor W. Hänsch, and Jakob Reichel, Coherence in Microchip Traps, Phys. Rev. Lett. **92**, 203005 (2004).

[15] T. P. Meyrath et al., Bose-Einstein condensate in a box, Phys. Rev. A **71**, 041604(R) (2005).

[16] Wojciech H. Zurek, Decoherence and the transition from quantum to classical – REVISITED, Progress in Mathematical Physics **48**, 1 (2007); quant-ph/0306072 (2003).

[17] Long coherence times of internal degrees of freedom have been seen very close to classical objects such as ion chips and atom chips [e.g. P. Treutlein et al., Phys. Rev. Lett. **92**, 203005 (2004)]. While to date, no direct measurement has been done of the single particle spatial coherence time in these systems, the heating rates observed in ion chips suggest that the spatial coherence time is short [N. Daniilidis et al., New J. of Phys. **13**, 013032 (2011)].

[18] Yoav Sagi, Ido Almog, and Nir Davidson, Process Tomography of Dynamical Decoupling in a Dense Cold Atomic Ensemble, Phys. Rev. Lett. **105**, 053201 (2010).

[19] Yoav Sagi, Ido Almog, and Nir Davidson, Universal Scaling of Collisional Spectral Narrowing in an Ensemble of Cold Atoms, Phys. Rev. Lett. **105**, 093001 (2010).